Comparative Study of Coaxial Main Rotor Aerodynamics at Forward Flight Based on Free Wake Model and Unsteady Reynolds-Averaged Navier–Stokes Method

Sergey Gennadievich Konstantinov[1] iD, Yuri Mikhailovich Ignatkin[1] iD, Pavel Viacheslavovich Makeev[1] iD, Alexander Ivanovich Shomov[1] iD, Sergey Olegovich Nikitin[1,*] iD

1. Moscow Aviation Institute ROR – National Research University – Aeronautical Engineering – Moscow – Russian Federation.

*Correspondence author: luber6785@yandex.ru

ABSTRACT

This paper is dedicated to the numerical modeling of the aerodynamic characteristics of the full-scale coaxial main rotor. The modes of forward flight in the range of values V = 30−60 m·s⁻¹ (108−216 km·h⁻¹) have been under consideration. The simulation has been performed with the usage of two computational fluid dynamics (CFD) approaches: the free wake model (FWM) developed by the authors and the unsteady Reynolds-averaged Navier–Stokes (URANS) equations method based on the Ansys Fluent software. The coefficients of rotor thrust and torque, vortex wake shapes and induced velocity fields have been obtained and analyzed. The FWM and the URANS modeling data match satisfactorily. The FWM demonstrates a significant advantage in computing time and resources costs with sufficient accuracy in resulting rotor's basic aerodynamic characteristics. That's why it seems appropriate to use the FWM for preliminary simulations, taking into account before using the high time and resource intensive the URANS method for comprehensive investigation of coaxial rotor aerodynamics at forward flight modes.

Keywords: Coaxial main rotor; Forward flight; CFD; URANS; Free wake model.

INTRODUCTION

Aerodynamics of the helicopter's main rotor at forward flight has a number of features. At the forward flight with low and medium speeds, the vortex wake structures behind the rotor are very complex. The wake behind the rotor collapses into the right and left *supervortexes* structures (Leishman 2006). They have a high intensity and largely determine the induced velocities field around the rotor. The blade-vortex interaction phenomena have also great influence on the rotor aerodynamic at the forward flight (Leishman 2006). The high-speed forward flight is connected with retreating blade stall and advancing blade tip transonic flow, which limit the flight speed of conventional helicopters (Leishman 2006).

Separately, it is possible to distinguish the coaxial rotors, consisting of two rotors rotating over one axis in different directions with spaced rotational planes. A special feature of the coaxial rotors is also a complex aerodynamic interaction between the upper (UR) and lower (LR) rotor (Leishman 2006; Petrosian 2004).

The coaxial scheme has been the basis of Kamov helicopters since the 1950s, from the Ka-8 (1949) to the Ka-52 (1997) (Petrosian 2004). In 1970s, due to its unique properties, coaxial main rotor has formed the basis of the advanced blade concept (ABC) technology (Ruddell 1977). Using ABC, the Sikorsky S-69 (1972) and Sikorsky X-2 (2008) helicopter technology demonstrators and prototypes of Sikorsky S-97 (2015) and Sikorsky-Boeing SB-1 Defiant (2019) high-speed helicopters have been designed. With the development of the ABC technology, research in the field of coaxial main rotor aerodynamics has become particularly widespread.

To study the helicopter rotor aerodynamics, modern methods of computational fluid dynamics (CFD) are widely used. Herewith, modeling the coaxial rotor aerodynamics is characterized by increased complexity. Various vortex methods (Feil *et al.* 2018; Kritsky *et al.* 2020; Kwon *et al.* 2021; Singh and Friedmann 2020; Tan *et al.* 2018), finite volume methods (FVM) (Deng *et al.* 2019; Jia and Lee 2021; Kim and Brown 2010; Klimchenko *et al.* 2017; Park and Kwon 2021; Passe *et al.* 2015; Qi *et al.* 2017; 2019; Wang *et al.* 2020) and coupled combined methods (Egolf *et al.* 2010; Linton *et al.* 2018) are currently used to model the aerodynamics of coaxial main rotor at forward flight. When solving problems of rotor aerodynamics with the FVM, the URANS method with different models of turbulence is usually used (Deng *et al.* 2019; Jia and Lee 2021; Park and Kwon 2021; Qi *et al.* 2017; 2019; Wang *et al.* 2020) It should be noted that most of researches (Deng *et al.* 2019; Feil *et al.* 2018; Klimchenko *et al.* 2017; Kwon *et al.* 2021; Linton *et al.* 2018; Qi *et al.* 2017; 2019) are currently aimed at modeling the coaxial rotor aerodynamics at the high values of flight speeds corresponding to the advance ratio values of $\mu = V \cdot \cos\alpha_R / \omega R = 0.3 - 0.5$ and higher (V is the flight speed; α_R is the angle of attack of the rotor; ωR is the speed of rotation of the blade tips). This is due to the great interest to the use of coaxial rotor as a lift system for high-speed helicopters according to the ABC scheme, flying at speeds of 400–500 km·h^{-1} and higher. As a source of horizontal propulsion in such helicopters, a pushing propeller (X-2, S-97, SB-1 Defiant) is usually used. At the same time, the classic Kamov Company coaxial helicopters, such as the Ka-32 and the Ka-226, have maximum forward flight speeds of 220–260 km·h^{-1} which correspond to the values of $\mu \approx 0.3$, and use the main rotor itself as a source of horizontal propulsion.

Presented work considers the aerodynamic characteristics of coaxial main rotor of Ka-226 helicopter at forward flight with different speeds: from a low power costs flight speed V = 30 m·s^{-1} = 108 km·h^{-1} ($\mu \approx 0.15$) to the cruising flight speed V = 60 m·s^{-1} = 216 km·h^{-1} ($\mu \approx 0.3$).
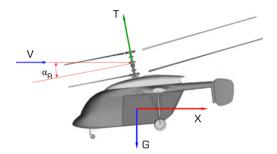
The study has been performed using two modern CFD methods: original free wake model (FWM) developed by the authors (Ignatkin *et al.* 2009) and the URANS method based on the Ansys Fluent software. Previously, these approaches had been used and validated by the authors in comparative numerical studies of helicopter rotor aerodynamics at the different flight modes. The cases having been under consideration: conventional rigid model-scale rotor at hover and forward flight in the range of $\mu = 0.1 - 0.45$ (Konstantinov *et al.* 2020); full-scale coaxial main rotor at hover (Ignatkin *et al.* 2021). Thus, this present work is a continuation and development of the mentioned researches.

As a result of the research, new data on the aerodynamics of the full-scale coaxial main rotor of a classical coaxial helicopter in a wide range of forward flight speeds has been obtained. Final materials include: high-resolution visualizations data of vortex wake structure, induced velocity fields in the wake behind the rotor, dependencies of the rotor thrust and torque on time (total value and UR/LR separately). Comparing the results obtained on the both FWM/URANS approaches has allowed analyzing their capabilities, evaluating advantages and disadvantages and performing mutual validation.
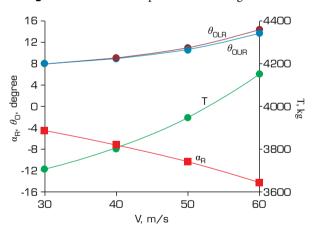
THE OBJECT OF STUDY AND ASSUMPTIONS

The paper considers an isolated coaxial main rotor of the Ka-226 helicopter (Bourtsev *et al.* 2007; Konstantinov *et al.* 2021; Vassiliyev *et al.* 2007), consisting of URs and LRs rotating in different directions. The coaxial rotor has the following characteristics: number of blades $N_b = 6$ (3 + 3), rotor solidity $\sigma = 0.075$, blade tip speed $\omega R = 198$ m·s^{-1}, blade twist $\theta_{tw} = -8.35°$, blade chord $b = 0.26$ m, rotor radius R = 6.62 m, distance between UR/LR rotational plane h = 1.142 m.

Comparative Study of Coaxial Main Rotor Aerodynamics at Forward Flight Based on Free Wake Model and Unsteady Reynolds-Averaged Navier–Stokes Method

3

Modeling of the coaxial rotor aerodynamics has been performed at horizontal flight modes with speeds V = 30, 40, 50, 60 m·s⁻¹ ($\mu \approx 0.15$; 0.2; 0.25; 0.3). These velocities correspond to the Mach numbers at the tip of advancing blade M_{AT} = 0.67; 0.7; 0.73 and 0.76. Used rotor setup parameters such as: angles of attack of the rotor α_R and UR/LR collective and cyclic pitch law have been corresponded to the flight of Ka-226 helicopter (Fig. 1) with take-off weight of G = 3600 kg. Simulation of rotor aerodynamics has been performed in an isolated setting, but rotor setup parameters have covered the helicopter fuselage aerodynamic loads (drag and lift). Rotor setup parameters including rotor blades flapping had been calculated earlier using the FWM. Figure 2 shows precalculated dependences of required rotor's angle of attack α_R, required URs/LRs' collective pitch θ_0 angles and rotor thrust T values on the flight speed values V. Required rotor thrust values are growing with increasing flight speed values. This is due to the need to compensate the fuselage aerodynamic loads. The aerodynamic characteristics of the fuselage had been obtained earlier by numerical modeling based on the URANS method and validated by the experimental data (Ignatkin and Konstantinov 2017). Rotor setup and control parameters have ensured the required rotor total thrust force T and UR/LR torque balancing. Precalculated rotor setup and control data from FWM have been used further in the URANS calculations.

Source: Elaborated by the authors.

Figure 1. Ka-226 helicopter at forward flight mode.

Source: Elaborated by the authors.

Figure 2. Calculated dependences of coaxial rotor thrust force T, angle of attack α_R and collective pitch θ_0 values vs. forward flight speed V.

The descriptions of the FWM and the URANS method used for numerical study are given below.

FREE WAKE MODEL

The FWM developed at the Helicopter Design Department of Moscow Aviation Institute is based on the lifting line theory and the blade element theory. Each blade element is modeled by an attached vortex segment located on a quarter of the blade element chord c (see Fig. 3) with the control point in the center of the segment. For each time step Δt a quadrangular contour

consisting of vortex segments with a constant circulation Γ, equal to the attached vortex circulation, descends from the blade element. The circulation of the attached vortex changes along the blade radius and depends on the blade azimuthal position. Attached vortex circulation is determined with an iterative method. The coefficients of the lift force c_L and the drag force c_D of the blade element are determined at the found angle of attack α and the total flow velocity W based on airfoil steady test data in wind tunnel. The system of vortex contours creates a free vortex wake in the form of a grid of longitudinal and transverse vortex segments (Fig. 3). The vortex wake grid is deformed at each calculated step under the influence of external and induced velocity fields. A key part of the model is calculation of induced velocities from the vortex segment which is an element of the free vortex wake grid. The described model uses an approach that allows determining the vorticity field from the vortex segment and the induced velocity from this vorticity field on the basis of an exact solution of the vortex source diffusion. The model with its basic equations is described in detail in previous works (Ignatkin *et al.* 2009; Konstantinov *et al.* 2021).
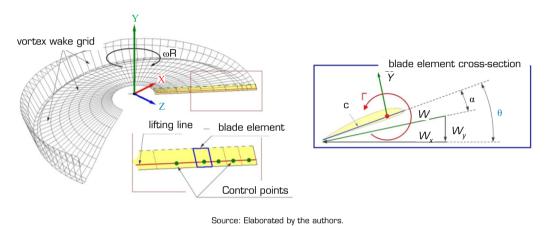

Source: Elaborated by the authors.

Figure 3. Free wake model.

Computational model of the Ka-226 helicopter coaxial main rotor at forward flight modes is shown in Fig. 4. Each of the rotor blades has consisted of 12 calculated elements. The calculated azimuth step was Δψ = 6°. For each flight mode up to 10 rotor revolutions have been calculated. Calculation of one task using a personal computer equipped with 8 cores (16 threads) has taken about 12 h.
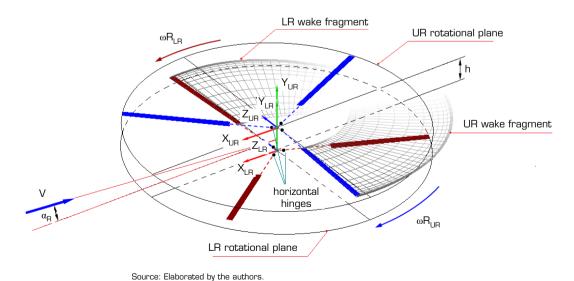

Source: Elaborated by the authors.

Figure 4. Calculation model of the coaxial rotor under study.

Comparative Study of Coaxial Main Rotor Aerodynamics at Forward Flight Based on Free Wake Model and Unsteady Reynolds-Averaged Navier–Stokes Method

5

UNSTEADY REYNOLDS-AVERAGED NAVIER–STOKES METHOD

Figure 5 shows a 3D model of the Ka-226 helicopter coaxial main rotor used for the URANS method of aerodynamic study. The computational mesh has had a block-structured topology, containing about 30 million hexahedral cells. The total number of cells in various works when modelling coaxial rotor aerodynamics usually lies in the range of 10-20 million (Deng *et al.* 2019; Jia and Lee 2021; Park and Kwon 2021; Qi *et al.* 2017; 2019; Wang *et al.* 2020). A higher resolution of the computational mesh in particular allows obtaining high-quality rotor wake structures visualizations. The upper and lateral boundaries of computational domain have been located at a distance of 2.5 R from the rotor model, the lower boundary at a distance of 3 R, and the boundary of the flow output at a distance of 7 R (Fig. 6). In the presented study the overset mesh method has been used. The computational mesh consisted of six zones of the blades and two zones of the external flow region with different mesh density (Fig. 6). At the boundaries of the blade zones the overset interface has been used. Nowadays the overset meshes are widespread for helicopter rotor aerodynamics modeling (Klimchenko *et al.* 2017; Qi *et al.* 2017; 2019) with taking into account the rotor blade flapping motions. At the upper and lateral boundaries of the computational domain, the boundary condition of the Pressure IN flow input has been set. At the lower and output boundaries of the computational domain, the Pressure OUT boundary condition has been set.
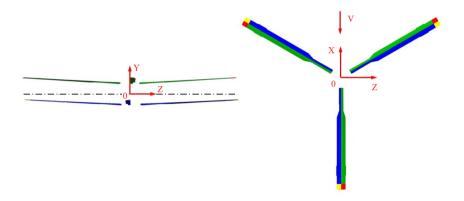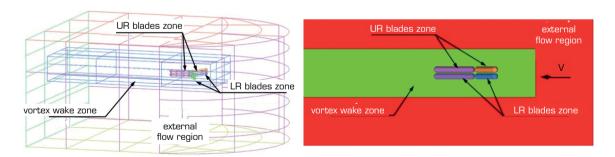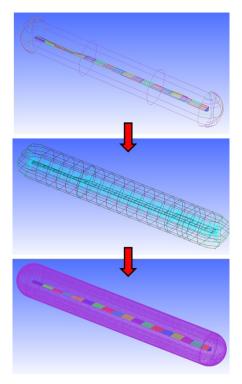

Source: Elaborated by the authors.

Figure 5. Model of coaxial main rotor.

Source: Elaborated by the authors.

Figure 6. Structure of computational volume mesh.

Each rotor blade has been divided into 20 equal sections (chambers) along the radius (Fig. 7). For a more accurate simulation of the aerodynamic characteristics, the computational mesh has been adapted to the specificity of the flow around the blades and has had an increased number of cells in the root and tip sections of the blades (Fig. 8). The mesh of each blade has had 2.1 million cells. Thus, the total mesh of 6 blades has contained 12.6 million cells. The cross section of the blade mesh has had a diameter equal to 4.5 blade chord (Fig. 9). Near the blade surface the computational mesh has been built in such a way that the first node of the mesh has been located in the area of the viscous velocity profile $Y+ \leq 1$.

Source: Elaborated by the authors.

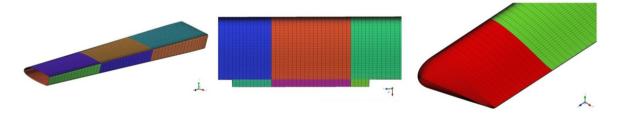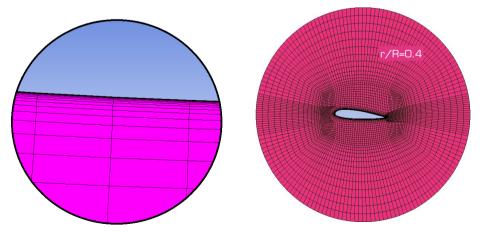**Figure 7.** Structure of computational volume mesh around the blade.

Source: Elaborated by the authors.

Figure 8. Surface mesh at the blade tip.

Source: Elaborated by the authors.

Figure 9. Structure of the mesh in the blade cross section.

Comparative Study of Coaxial Main Rotor Aerodynamics at Forward Flight Based on Free Wake Model and Unsteady Reynolds-Averaged
Navier–Stokes Method

7

Numerical simulation has been performed in unsteady setting taking into account the changing in the flow parameters over time. To describe of a viscous turbulent flow of compressible gas, the Reynolds-averaged Navier–Stokes equations closed by the k-ω SST turbulence model have been used (Menter 1993).

The parameters of the initial turbulence have been selected basing on the conditions of the average intensity of the developed turbulent flow. The relative turbulent viscosity has been assumed to be 5. The value of the turbulent intensity has been assumed to be 1%.

Preliminary calculations aimed at studying the grid convergence had showed that selected parameters of the computational mesh were sufficient for reliable calculation the aerodynamic characteristics of the studied coaxial rotor.

The calculation of a single mode has taken about 7 days using a high-performance supercomputer cluster equipped with 360 computing cores.

RESULTS AND DISCUSSION

Figure 10 shows the calculated dependences of the time-averaged rotor thrust c_T (Fig. 10a) and torque c_Q (Fig. 10b) coefficients on the forward flight speed V. The thrust coefficient is related to the rotor thrust force T by the equation: $c_T = (2T)/(\rho(\omega R)^2 \pi R^2)$, and the torque coefficient with the rotor torque moment Q through the equation: $c_Q = (2Q)/(\rho(\omega R)^2 \pi R^3)$. Figure 10 shows separated and total values of the UR/LR thrust coefficients. Data obtained on the basis of the FWM/URANS calculations are in good agreement with each other over the considered range of V values. It can be seen that the values of UR/LR thrust and torque coefficients at forward flight are equal, and this fact has also been noted in the works of the other authors (Kwon *et al.* 2021; Passe *et al.* 2015; Wang *et al.* 2020). The obtained results confirm the applicability of used methods for estimating the total aerodynamic characteristics of a coaxial rotor at forward flight modes.
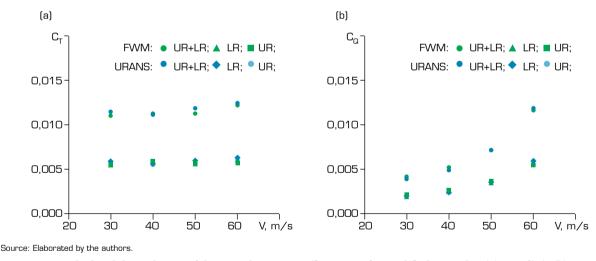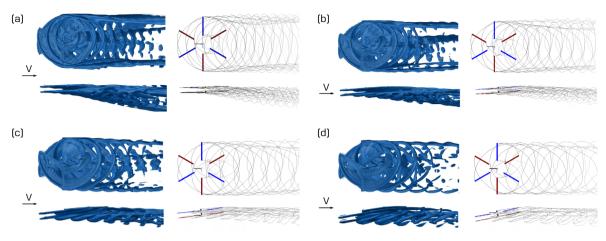

Source: Elaborated by the authors.

Figure 10. Calculated dependences of thrust and torque coefficients on forward flight speed V. (a) $c_T = f(V)$; (b) $c_Q = f(V)$.

Figure 11 shows the results of vortex wake visualizations behind the rotor based on the FWM/URANS approaches. The URANS-based rotor wake visualizations are performed using isosurfaces for a fixed vorticity $\omega = 15$ s^{-1}. Such method of a wake visualization gives good results (Ignatkin *et al.* 2020; Kim and Brown 2010; Konstantinov *et al.* 2021; Linton *et al.* 2018; Passe *et al.* 2015) in the case of sufficient resolution of the calculated mesh (in the presented work, mesh has contained about 30 million elements). The rotor wake visualizations based on the FWM show the vortices coming off the blade tip and root sections. This technique makes it easier to analyze the main part of vortex wake structure. A comparison of the vortex wake structures obtained on the FWM/URANS presented in Fig. 11 shows a good agreement.

Figure 11. Calculated visualizations of the vortex wake of the coaxial rotor at forward flight. (a) V = 30 m·s⁻¹;
α_R = –4.7°; (b) V = 40 m·s⁻¹; α_R = –7.3°; (c) V = 50 m·s⁻¹; α_R = –10.4°; (d) V = 60 m·s⁻¹; α_R = –14.4°.

A large amount of data on the visualization of the structure of the vortex wake behind the full-scale coaxial rotor in hovering and forward flight modes has been obtained using smoke visualization during flight experiments conducted on the basis of the Ka-32 helicopter by Kamov Company and Gromov Flight Research Institute in 1993 (Akimov *et al.* 1994; Bourtsev *et al.* 2001). The main features of the formation of a wake behind the coaxial rotor are observed for FWM/URANS data in Fig. 11. In particular, at forward flight speeds V = 30 m·s⁻¹ (Fig. 11a) and V = 40 m·s⁻¹ (Fig. 11b), it is clearly visible that the vortex wake collapses into the right and left *supervortexes*. With an increase in the flight speed, the vortex wake has less deformed, since the velocities of the incoming flow V have been significantly higher than induced velocities. From Fig. 11c (V = 50 m·s⁻¹) and Fig. 11d (V = 60 m·s⁻¹) it follows that the vortex wake shapes obtained on the FWM/URANS also coincide.

In addition to visualizing the vortex wake structures, the calculation of the induced velocity fields in the wake behind the rotor has been performed. This made it possible to compare the accuracy of the vortex wake modeling by the FWM/URANS through a comparative analysis of the calculated induced velocity profiles. The induced velocity profiles have been constructed in the associated coordinate system of the coaxial rotor (see Fig. 12) in the projection on the OY axis along the control lines located in the rotor wake at distances X/R = –0.5; –1.0; –1.5 and lying in the rotational plane of the LR (Y/R = 0). For the URANS method, induced velocity profiles have been calculated by determining the vertical projection of the velocity vector in the computational mesh cells through which the control lines have passed. For the FWM, the vertical projections of the induced velocity have been determined by the influence of the vortex wake behind the rotors.
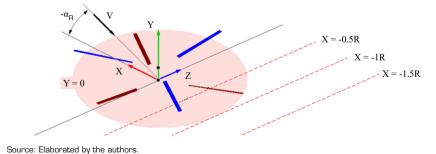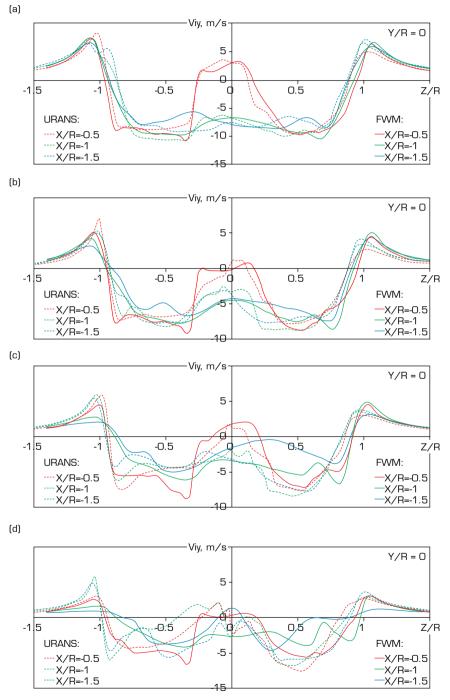
Figure 12. Scheme of measurement lines for the induced velocity profiles analysis.

The diagrams of the induced velocities are shown in Fig. 13. It can be seen that at V = 30 m·s⁻¹ (Fig. 13a) and V = 40 m·s⁻¹ (Fig. 13b) induced velocity profiles calculated on the basis of the FWM and the URANS method coincide well. At V = 50 m·s⁻¹ (Fig. 13c) the degree of coincidence for the profile at the distance X/R = –1.5 deteriorates. For V = 60 m·s⁻¹ the match remains satisfactory only for the profile at the distance X/R = –0.5 (Fig. 13d). The obtained results indicate sufficient accuracy of the simulation based on the FWM of both near and far vortex wake in the range V = 30–40 m·s⁻¹. At the same time, the dependences c_T = f(V) and c_Q = f(V) shown in Fig. 10 coincide well for both FWM/URANS methods over the entire forward flight speed range V. This can be explained by the fact

Comparative Study of Coaxial Main Rotor Aerodynamics at Forward Flight Based on Free Wake Model and Unsteady Reynolds-Averaged Navier–Stokes Method

9

that aerodynamic loads depend mainly on the induced influence of the vortices located near the rotational plane of the blades. From the induced velocity profiles shown in Fig. 13, it is also possible to note the symmetry of the obtained velocity profiles relative to the OY axis. This feature is a property of the coaxial rotor and is not observed for conventional rotor (Ignatkin *et al.* 2020). In addition, in the central part of the profiles (−0.25 < z/R < 0.25) here is an intensive upwards flow (Fig. 13a). That is obviously caused by vortices coming off the blades' roots. This vortex structure is observed on the URANS-visualization between the left and right *supervortexes* (Fig. 11a).

Source: Elaborated by the authors.

Figure 13. Profiles of induced velocities in the rotor wake at forward flight. (a) V = 30 m·s^{-1}; α_R = −4.7°; (b) V = 40 m·s^{-1}; α_R = −7.3°; (c) V = 50 m·s^{-1}; α_R = −10.4°; (d) V = 60 m·s^{-1}; α_R = −14.4°.

Figure 14 shows the dependences of the instantaneous values of the thrust c_T and the torque c_Q coefficients of the coaxial rotor on the number of revolutions n, obtained on the basis of the FWM/URANS methods. Total thrust ($c_T = c_{TUR} + c_{TLR}$) and torque ($c_Q = c_{QUR} + c_{QLR}$) curves and separated UR and LR curves are presented. The time-averaged values of the c_T and c_Q coefficients are presented in Fig. 10.

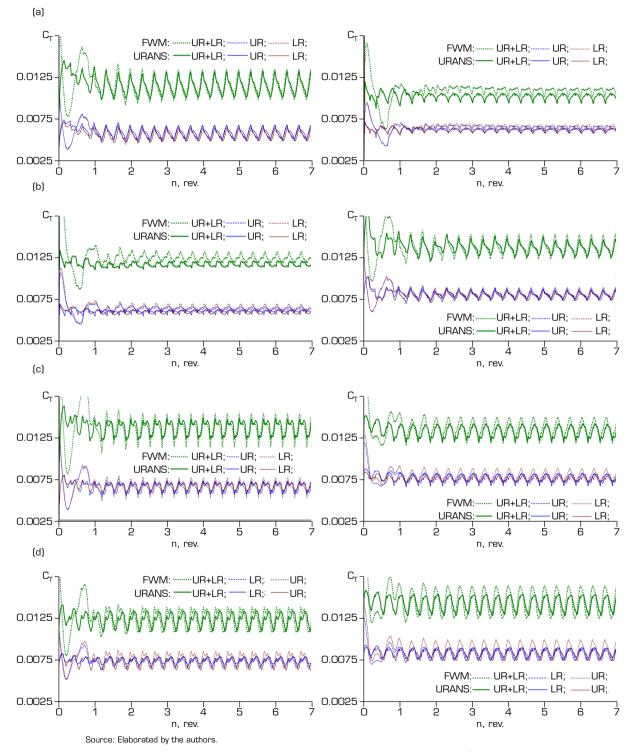Source: Elaborated by the authors.

Figure 14. Calculated dependences of instantaneous thrust and torque coefficients vs. number of rotor revolutions based on the FWM and the URANS. (a) V = 30 m·s⁻¹; α_R = –4.7°; (b) V = 40 m·s⁻¹; α_R = –7.3°; (c) V = 50 m·s⁻¹; α_R = –10.4°; (d) V = 60 m·s⁻¹; α_R = –14.4°.

Comparative Study of Coaxial Main Rotor Aerodynamics at Forward Flight Based on Free Wake Model and Unsteady Reynolds-Averaged Navier–Stokes Method

11

For all the forward flight speeds $V = 30; 40; 50; 60$ m·s^{-1}, the calculated diagrams on the Fig. 14 demonstrates pulsations of the thrust and torque coefficients over time. These pulsations are mainly associated with the periodic passage of the UR and LR blades over each other, and their frequency depends on the number of blades. At the $V = 30$ m·s^{-1}, the amplitude of thrust pulsations is maximal and reaches 33% of the mean value (FWM) and up to 25% of the mean value (URANS). At the higher flight velocities thrust pulsation amplitudes decreases to 26% at $V = 40$ m·s^{-1} (Fig. 14b) (FWM) and to 15% at $V = 50$ m·s^{-1} (Fig. 14c) (URANS). Similar pulsations of thrust and torque are characteristics of the coaxial rotors (Kim and Brown 2010; Konstantinov *et al.* 2021; Kritsky *et al.* 2020). It should be noted that for $c_T = f(n)$ diagrams, in general, there is a better match between the FWM and URANS calculations than for $c_Q = f(n)$ diagrams. It can also be seen that diagrams of $c_T = f(n)$ have the best matching at $V = 30$ m·s^{-1} (Fig. 14a) and $V = 40$ m·s^{-1} (Fig. 14b), and for diagrams of $c_Q = f(n)$ at $V = 50$ m·s^{-1} (Fig. 14c) and $V = 60$ m·s^{-1} (Fig. 14d).

From the above-mentioned results, it can be concluded that both methods allow obtaining with a certain accuracy the pulsations of the aerodynamic characteristics of the coaxial main rotor connected with the aerodynamic interference between UR and LR blades. The results shown in Fig. 14 also confirm the good quality of the computational mesh developed for the URANS method.

CONCLUSIONS

On the basis of the FWM and the URANS method, numerical simulation of the aerodynamic characteristics of full-scale coaxial main rotor of the Ka-226 helicopter in forward flight in the speed range of $V = 30$–60 m·s^{-1} ($\mu \approx 0.15$–0.3) has been performed.

The comparison of calculated rotor thrust and torque coefficients has showed a good match for both FWM/URANS calculations methods. Due to the high resolution of the used UFWM/URANS methods the detailed vortex wake visualizations data has been obtained. Comparison of the FWM/URANS wake visualizations data has showed good agreement. The main features of the structures of a vortex wake behind the rotor at forward flight including forming of *supervortexes* structures have been obtained and analyzed. On the base of the FWM/URANS methods the induced velocity fields in the wake behind the rotor have been calculated and compared. The features of the coaxial rotor have been analyzed including the induced velocity profiles symmetry with respect to the OY axis and the intense upward flow in the central part behind the rotor. The induced velocity fields data obtained on the basis of the FWM/URANS match well at forward flight speeds $V = 30$–40 m·s^{-1}, and match satisfactorily at $V = 50$ m·s^{-1}.

The obtained experience of using the FWM and URANS methods for comparative modeling of a coaxial rotor aerodynamics at forward flight allowed making the following conclusions. The FWM provides the calculation of the main aerodynamic characteristics of the coaxial rotor at the considered range of forward flight speeds with low computational and time costs and sufficient accuracy. The URANS, as a higher-level method, requires significant computational resources and preparing time costs. At the same time, the URANS method provides wide possibilities for a fine and deep study of physical processes of rotor aerodynamics, including the simulation of the complex spatial flow around the blades, pressure distribution over blades surfaces analysis, accurate accounting of the blade-vortex interactions, possibility of an aeroacoustics investigations.

Thus, the studies have demonstrated the high effectiveness of using the FWM for a fast evaluation of the total aerodynamic forces on the rotor, as well as for preliminary calculating the initial data for the URANS method. This approach may significantly reduce the cost of time and computational resources during comprehensive investigation of the coaxial rotor aerodynamics of classical helicopters.

AUTHORS' CONTRIBUTION

Conceptualization: Ignatkin YM; **Methodology:** Konstantinov SG, Makeev PV and Shomov AI; **Investigation:** Konstantinov SG, Makeev PV; **Writing — original draft:** Makeev PV and Konstantinov SG; **Writing — review & editing:** Ignatkin YM, Makeev PV and Nikitin SO; **Resources:** Konstantinov SG; **Supervision:** Nikitin SO.

DATA AVAILABILITY STATEMENT

The data will be available upon request.

FUNDING

ACKNOWLEDGEMENTS

REFERENCES

Akimov AI, Butov VP, Bourtsev BN, Selemenev SV (1994) Flight Investigation of Coaxial Rotor Tip Vortex Structure. Paper presented AHS 50th Annual Forum. Washington, District of Columbia, United States of America. [accessed Feb 14 2022]. https://vtol.org/store/product/flight-investigation-of-coaxial-rotor-tip-vortex-structure-578.cfm

Bourtsev BN, Ryabov VI, Selemenev SV (2007) Mathematical modeling of Ka-226 / Ka-26 helicopter main rotor blade flapping motion at rotor acceleration / deceleration in wind conditions. Paper presented 33rd European Rotorcraft Forum. Kazan, Russia. [accessed Feb 14 2022]. https://dspace-erf.nlr.nl/xmlui/bitstream/handle/20.500.11881/221/Mathematical%20modeling%20of%20Ka-226%20%20Ka-26%20helicopter.pdf?sequence=1&isAllowed=y

Bourtsev BN, Ryabov VI, Selemenev SV, Butov VP (2001) Helicopter Wake Form Visualization Results and their Application to Coaxial Rotor Analysis at Hover. Paper presented 27rd European Rotorcraft Forum. Moscow, Russia.

Deng J, Fan F, Liu P, Huang S, Lin Y (2019) Aerodynamic characteristics of rigid coaxial rotor by wind tunnel test and numerical calculation. Chinese J Aeronaut 32(3):568-576. https://doi.org/10.1016/j.cja.2018.12.026

Egolf TA, Rajmohan N, Reed E, Sankar L (2010) A Hybrid CFD Method for Coaxial Rotor Performance Prediction in Forward Flight, Paper presented AHS Aeromechanics Specialists Conference on Aeromechanics. AHS; San Francisco, California, United States of America.

Feil R, Rauleder J, Cameron CG, Sirohi J (2018) Aeromechanics Analysis of a High-Advance-Ratio Lift-Offset Coaxial Rotor System. J Aircrt 56(1):1-13. https://doi.org/10.2514/1.C034748

Ignatkin YM, Konstantinov SG (2017) [Researches of aerodynamic characteristics of planer helicopters using CFD-method. All-Russian Scientific-Technical Journal "Polyot" ("Flight")]. 9-10:34-41. [accessed Feb. 14 2022] http://www.ros-polet.ru/files/archiv/pl_9-10_2017_web.pdf. Russian.

Ignatkin YM, Makeev PV, Grevtsov BS, Shomov AI (2009) A nonlinear blade vortex propeller theory and its applications to estimate aerodynamic characteristics for helicopter main rotor and anti-torque rotor. Aerospace MAI Journal 16(5):24-31.

Ignatkin YM, Makeev PV, Konstantinov SG, Shomov AI (2020). Modelling the helicopter rotor aerodynamics at forward flight with free wake model and URANS method. Aviation 24(4): 149-156. https://doi.org/10.3846/aviation.2020.12714

Jia Z, Lee S (2021) Aerodynamically induced noise of a lift-offset coaxial rotor with pitch attitude in high-speed forward flight. J Sound Vib 491:115737. https://doi.org/10.1016/j.jsv.2020.115737

Comparative Study of Coaxial Main Rotor Aerodynamics at Forward Flight Based on Free Wake Model and Unsteady Reynolds-Averaged Navier–Stokes Method

13

Kim HW, Brown RE (2010) A Comparison of coaxial and conventional rotor performance. J Am Helicopter Soc 55(1):12004. https://doi.org/10.4050/JAHS.55.012004

Klimchenko V, Sridharan A, Baeder JD (2017) CFD/CSD Study of the Aerodynamic Interactions of a Coaxial Rotor in High-Speed Forward Flight. Paper presented 35th AIAA Applied Aerodynamics Conference. AIAA; Denver, Colorado, United States of America. https://doi.org/10.2514/6.2017-4454

Konstantinov SG, Ignatkin YM, Makeev PV, Nikitin SO (2021) Comparative study of coaxial main rotor aerodynamics in the hover with the usage of two methods of computational fluid dynamics. J Aerosp Technol Manag 13:e1821. https://doi.org/10.1590/jatm.v13.1210

Kritsky BS, Mirgazov RM, Anikin VA, Gerasimov OV (2020) Thrust pulsation of coaxial main rotor, caused by the blades relative position. Civil Aviation High Technologies 23(4):96-104. Russian. https://doi.org/10.26467/2079-0619-2020-23-4-96-104

Kwon Y-M, Park J-S, Wie S-Y, Kang HJ, Kim D-H (2021) Aeromechanics analyses of a modern lift-offset coaxial rotor in high-speed forward flight. Int J Aeronaut Space Sci 22:338-351. https://doi.org/10.1007/s42405-020-00300-8

Leishman JG (2006) Principles of Helicopter Aerodynamics. Cambridge: Cambridge University Press.

Linton D, Widjaja R, Thornber Ben (2018) Simulations of tandem and coaxial rotors using a CFD-coupled rotor model. Paper presented 21st Australasian Fluid Mechanics Conference. Adelaide, Australia. [accessed Jun 01 2021] https://people.eng.unimelb.edu.au/imarusic/proceedings/21/Contribution_781_final.pdf

Menter FR (1993) Zonal two equation k-ω turbulence models for aerodynamic flows. Paper presented 24th Fluid Dynamics Conference. AIAA; Orlando, Florida, United States of America. https://doi.org/10.2514/6.1993-2906

Park SH, Kwon OJ (2021) Numerical study about aerodynamic interaction for coaxial rotor blades. Int J Aeronaut Space Sci 22:277-286. https://doi.org/10.1007/s42405-020-00310-6

Passe BJ, Sridharan A, Baeden JD (2015) Computational Investigation of Coaxial Rotor Interactional Aerodynamics in Steady Forward Flight. Paper presented 33rd AIAA Applied Aerodynamics Conference. Dallas, TX. https://doi.org/10.2514/6.2015-2883

Petrosian ÈA (2004) Aerodynamics of coaxial helicopter. Moscow: Poligon-Press.

Qi H, Shi Y, Xu G, Huang S (2017) Analysis of aerodynamic interaction and trim characteristics of rigid coaxial rotor. Journal of Aerospace Power 32(12):3004-3012.

Qi H, Xu G, Lu C, Shi Y (2019) Computational investigation on unsteady loads of high-speed rigid coaxial rotor with high-efficient trim model. Int J Aeronaut Space Sci 20:16-30. https://doi.org/10.1007/s42405-018-0133-0

Ruddell AJ (1977) Advancing Blade Concept (ABC™) Development. J Am Helicopter Soc 22(1):13-23. https://doi.org/10.4050/JAHS.22.1.13

Singh P, Friedmann PP (2020) Aeroelastic stability analysis of hingeless coaxial rotors in hover and forward flight. Paper presented VFS Aeromechanics for Advanced Vertical Flight Technical Meeting. VFS; San Jose, California, United States of America.

Tan J, Sun Y, Barakos GN (2018) Unsteady loads for coaxial rotors in forward flight computed using a vortex particle method. Aeronaut J 122(1251):693-714. https://doi.org/10.1017/aer.2018.8

Vassiliyev BA, Kvokov VN, Pavlidi FN, Petrosian EA, Feofilov EB (2007) The Ka-226 helicopter flight performance and its compliance with the modern requirements. Paper presented 33rd European Rotorcraft Forum. Curran Associates; Kazan, Russia.

Wang B, Yuan X, Zhao Q-j, Zhu Z (2020) Geometry design of coaxial rigid rotor in high-speed forward flight. Int J Aerosp Eng 2020:6650375. https://doi.org/10.1155/2020/6650375